ISSN 0016-8521, Geotectonics, 2025, Vol. 59, No. 5, pp. 357–373. © Pleiades Publishing, Ltd., 2025.

Tectonic Position and Seismotectonic Manifestations of the March 28, 2025 Mandalay Earthquake $M_w = 7.7$ (Myanmar)

E. A. Zelenin[a], V. G. Trifonov[a], *, S. Yu. Sokolov[a], and D. M. Bachmanov[a]

[a] *Geological Institute, Russian Academy of Sciences, Moscow, 119017 Russia*

**e-mail: trifonov@ginras.ru*

Received June 16, 2025; revised August 10, 2025; accepted August 12, 2025

Abstract—The March 28, 2025 Mandalay Earthquake, with a magnitude $M_w = 7.7$ and its epicenter near the city of Mandalay, occurred within the zone of the major N–S-trending active right-lateral Sagaing Fault. The earthquake generated a seismic rupture zone that extended mainly southward from the epicenter along this fault. Using radar interferometry and subpixel correlation of satellite imagery, the authors determined the parameters of the rupture zone. Its length is ~460 km, with right-lateral displacement reaching the maximum observed amplitude of 5.8 m. Given the hypocentral depth of 10 km, the seismic ruptures can be considered the surface expression of the earthquake source. The Sagaing Fault is associated with the ophiolite belt of Myanmar, which represents relicts of the Mesotethys paleocean, displaced by Cenozoic tectonic movements. In northern Myanmar, where the Mandalay earthquake occurred, the ophiolite belt functions as the magmatic component of the submeridional northern segment of the Sunda island arc, beneath which the Indian Plate is subducting in the north-northeast direction. While the subduction surface is gently dipping near the front of the Sunda Plate, it experiences steep subduction further to the east. The Sagaing Fault lies above the eastern flank of the region of steep subduction of the Indian Plate. Beneath the region lies a mantle plume that reduces lithospheric thickness and causes softening of the lower crust. We suggest that the increased extent of the rupture zone of the Mandalay earthquake is due to the plasticity of the ophiolitic substrate, which facilitates rock slip, while the shallow depth of the hypocenter is related to the softening of the lower crust and upper mantle under the influence of the mantle plume. The significance of these factors is confirmed by comparing the Mandalay earthquake with the strongest earthquakes in Eastern Anatolia over the past 80 years, which occurred under similar tectonic conditions. These factors should be taken into account when assessing seismic impacts of major earthquakes.

Keywords: Mandalay earthquake, Sagaing Fault, Southeast Asia tectonics, seismogenic displacements, ophiolites, low-velocity mantle

DOI: 10.1134/S001685212570027X

INTRODUCTION

On March 28, 2025, at 06:20:54 UTC, a destructive earthquake with magnitude $M_w = 7.7$ occurred in Myanmar [68] (hereinafter referred to as the Mandalay earthquake) on the large right-lateral Sagaing Fault. Its epicentre was located near Mandalay (22°00′03″ N, 95°55′19″ E), the country's second largest city with a population of over 1 mln. The earthquake's hypocenter has been determined at a depth of 10 km [68], which allows us to expect the seismic rupture to have reached the surface. The earthquake was the strongest to hit mainland Southeast Asia since an earthquake with magnitude $M_s = 7.8$ struck the same fault in 1946 [57].

The aim of the article is to characterize the parameters of the seismic rupture, the tectonic position, and possible geodynamic nature of the earthquake that occurred. To date, evidence of the surface effects of the Mandalay earthquake has been extremely scant, and field work in the region has not been possible. Therefore, the study is based on deformation measurements using radar interferometry and subpixel correlation of high-resolution satellite images. The position of the earthquake source in the geological structure of the region was determined and compared with its deep structure, which was reconstructed using the UU-P07 seismic tomographic model [15, 31, 67].

MATERIALS AND METHODS

Geological Data

The structure of the part of Southeast Asia closest to the focal area of the Mandalay earthquake has been determined based on published data [10, 31, 48], which differ in the level of detail and scale of study and frequently contradict each other. In this study, we present what we believe to be the most probable model of the structure of the region, focusing on the details of the model that are important to assess the factors that determined the characteristics of the Mandalay earthquake. These factors were compared with the characteristics of the strongest East Anatolian earthquakes of the last 80 years using data from [8, 9, 11, 63].

Radar Interferometry

To determine the extent of the seismic rupture zone and magnitude of surface displacement, radar interferometry was used, which analyzes the phase difference of radio signals received by a receiver before and after seismic displacement of the relief.

The source of the data was radar images in the C-band obtained from the Sentinel-1 satellite [62]. Since the wavelength of C-band radio waves is approximately 5.6 cm, this method can map even small displacements with an amplitude of less than 1 m. To solve the formulated problems, radar images in the Interferometric Wide Swath (IW) mode with VV polarization were selected, covering the studied territory. The size of the baseline, i.e., the distance between survey points, did not exceed 100 m, and the interval between repeated surveys was 12 days. Image processing included selection of image pairs for the same area before and after the earthquake, their coregistration, calculation of interferograms, exclusion of the topographic component based on the SRTM 1 Arc-Second digital elevation model (DEM), filtering using the Goldstein algorithm [30], and phase unwrapping.

All processing stages are performed in the cloud software HyP3 (Hybrid Pluggable Processing Pipeline) with Vertex image search interface (Alaska State Science Center, USA). The calculated displacement values correspond to the direction towards or away from the satellite. To calculate the displacement along the fault plane, data on the vertical and horizontal angles of the direction to the satellite, given in the survey metadata, were used.

Subpixel Correlation of Optical Satellite Images

To determine the maximum values of horizontal displacements of the Earth's surface associated with the earthquake, the method of subpixel correlation of optical space images was additionally used. The initial data used were images from the Sentinel-2C satellite multi-spectral sensor MSI in the red spectrum zone with a spatial resolution of 10 m.

Paired images before and after the seismic event were selected, with minimal cloud cover and similar terrain illumination, with processing level L2 (radiometric correction and orthotransformation performed). Data processing and extraction of displacement vectors were done with the software tool autoRIFT (Automated Repeat Image Feature Tracking)—an automated algorithm for subpixel image matching that rejects points with low correlation [41].

Seismic Tomography

Currently, a detailed class of seismic tomography models has been created, calculated using teleseismic data with a spatial resolution of ~100 to ~50 km in seismically active zones, which significantly complements the understanding of the velocity structure of the mantle. In this study, we use the UU-P07 model [15, 31, 67], a specific feature of which is three-dimensional initial approximation of the velocity model, starting from which calculation and minimization of the residuals of the arrival times of seismic event signals at recording stations is performed.

As the initial approximation, researchers for a long time preferred radially symmetric PREM (Preliminary Reference Earth Model) [60], but by the end of the 2000s, most of the calculated models on low-frequency spherical harmonics up to $l = 20$ ceased to differ significantly [19]. This led to the introduction of three-dimensional initial approximations into practice [15], which significantly improved the quality of calculations of velocity variations and the computational results of the algorithms used.

The UU-P07 model features improved detail of δVp in the upper mantle in tectonically active segments of the lithosphere. The UU-P07 model in a user-friendly form is a three-dimensional matrix (cube) in space (X, Y, Z) with values δVp in each cell of the matrix. The cube sections are calculated along profiles with arbitrary trajectories in the (X, Y) plane, which are usually laid along and across the studied structures on the surface of the lithosphere.

TECTONIC ZONING OF INDOCHINA

The following tectonic zones have been identified in Myanmar and neighboring regions of India, Bangladesh, Thailand, Laos, Vietnam, and Yunnan Province in China (from west to east) [1, 5, 10, 48] (Fig. 1):

— Trough of the delta of the Ganges and Brahmaputra rivers;

— Indo-Burmese Ranges;

— Central Burma Trough;

— Sino-Burmese and Indosinian continental blocks.

Trough of the Delta of the Ganges and Brahmaputra Rivers

The 16–20-km-thick sedimentary cover of the Triassic–Quaternary deposits of the Neotethys and delta of its successor lies on thinned continental crust of the Indian Platform. In the eastern Bay of Bengal, the thickness of the cover can reach 30 km, of which at least 20 km are post-Eocene deltaic deposits [57].

Indo-Burmese Ranges

The ranges are a belt of meridionally elongated folds 1400 km in length (Fig. 2).

Most researchers consider this belt as an accretionary wedge in front of the magmatic part of the northern segment of the Sunda island arc. Their folds consist of Cretaceous and Paleogene rocks, deformed in the Late Oligocene and uplifted as ridges in the Middle Miocene [57]. Along the fold ridges there are faults

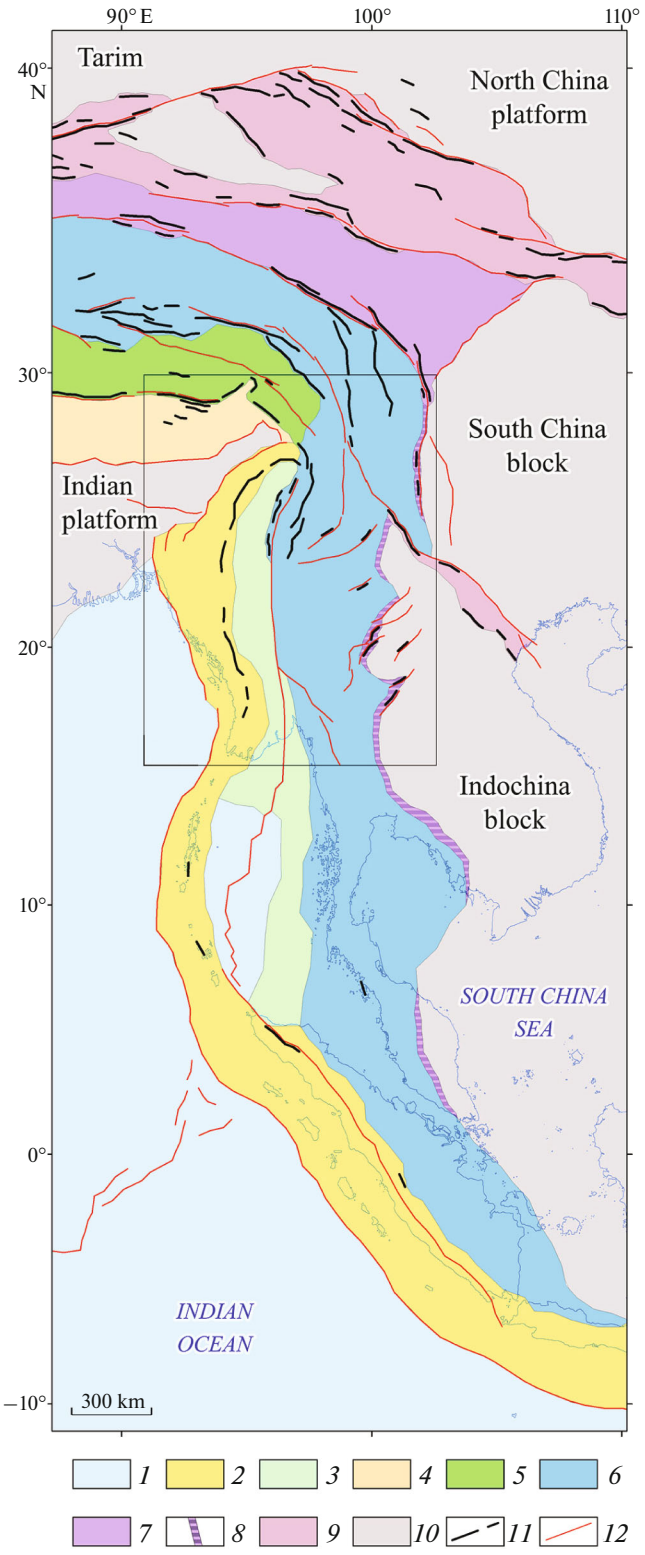

Fig. 1. Tectonic zones of Western Indochina (according to [1, 6, 10, 48]). Position of Fig. 2 is shown by rectangle. *1*, Areas of oceanic crust of Indian Plate; *2*, modern Sunda island arc; *3*, modern back-arc basin of Andaman Sea; *4*, area of Late Cenozoic deformations of Indian Platform (Himalayas); *5–7*, zones of sutures and active margins: *5*, Neotethys (Indus–Yarlung–Tsangpo zone and Lhasa block in Tibet); *6*, Mesotethys (Bangong–Nojiang suture and Qiangtang block in Tibet, ophiolite belt of Myanmar, Sino-Burmese block and their inferred southern continuations in Indochina); *7*, Paleotethys (Jinsha Suture and Songpan Block in Tibet); *8*, Paleotethys suture in Indochina; *9*, Hercynides; *10*, Early Paleozoic and Precambrian platforms and blocks; *11*, ophiolite outcrops; *12*, active faults.

with a dominant right-lateral displacement component (Fig. 3).

In the south of this zone, the 160-km-long Takhtay-Chaung fault shows right-lateral displacement of the interfluve by up to 11 km in the south of the fault and up to 5 km in the north. In the north of the tectonic zone, a right-lateral strike-slip fault of up to 3 km has been established along the 170-km-long Churachandpur-Mao fault [72]. To the east of it, on the boundary with the Central Burma Trough, is the Kabaw right-lateral oblique fault [49].

In the outer (western) part of the Indo-Burmese Range zone, the Tripura low-mountain fold belt is distinguished, 400 km in length, between the Shillong Plateau in the north and the coast of the Bay of Bengal in the south; it is featured by a less complex fold structure. The front of the Tripura fold belt has been shown to extend westward by 11 km over the last 2 Ma [57].

The Indo-Burmes Ranges are bounded in the north by the Shillong Plateau, a E–W elongated block of the continental lithosphere of the Indian Platform, rising 1 km above the surface of the delta and characterized by a crustal thickness of up to 35 km. The block is bounded by thrust faults dipping towards it. To the north is the Oldban Fault, buried under young sediments [21], and in the south, the active Dauki fault. Along it, the surface of Moho boundary under the plateau is raised by 6 km [57]. According to thermochronological data, the plateau began to rise 15–8 Ma ago [57].

Central Burma Trough

The trough is filled with Maastrichtian–Quaternary molasse-type deposits up to 10 km thick, and in the south, possibly up to 18 km. In the raised axial part of the trough, widening to the north, rocks of the metamorphic basement, ophiolites, and island-arc Pliocene–Quaternary volcanics are exposed, allowing this zone to be considered the magmatic part of the island arc. In the northern part of the trough, transpressive right-lateral deformations of the Upper Miocene–Quaternary deposits with the formation of an en echelon fold–thrust system have been identified [57]. Along the eastern edge of the trough extends the largest right-lateral strike-slip fault, the Sagaing (Fig. 3).

The rocks of the sedimentary cover of the Indo-Burmese Ranges are separated by a detachment sur-

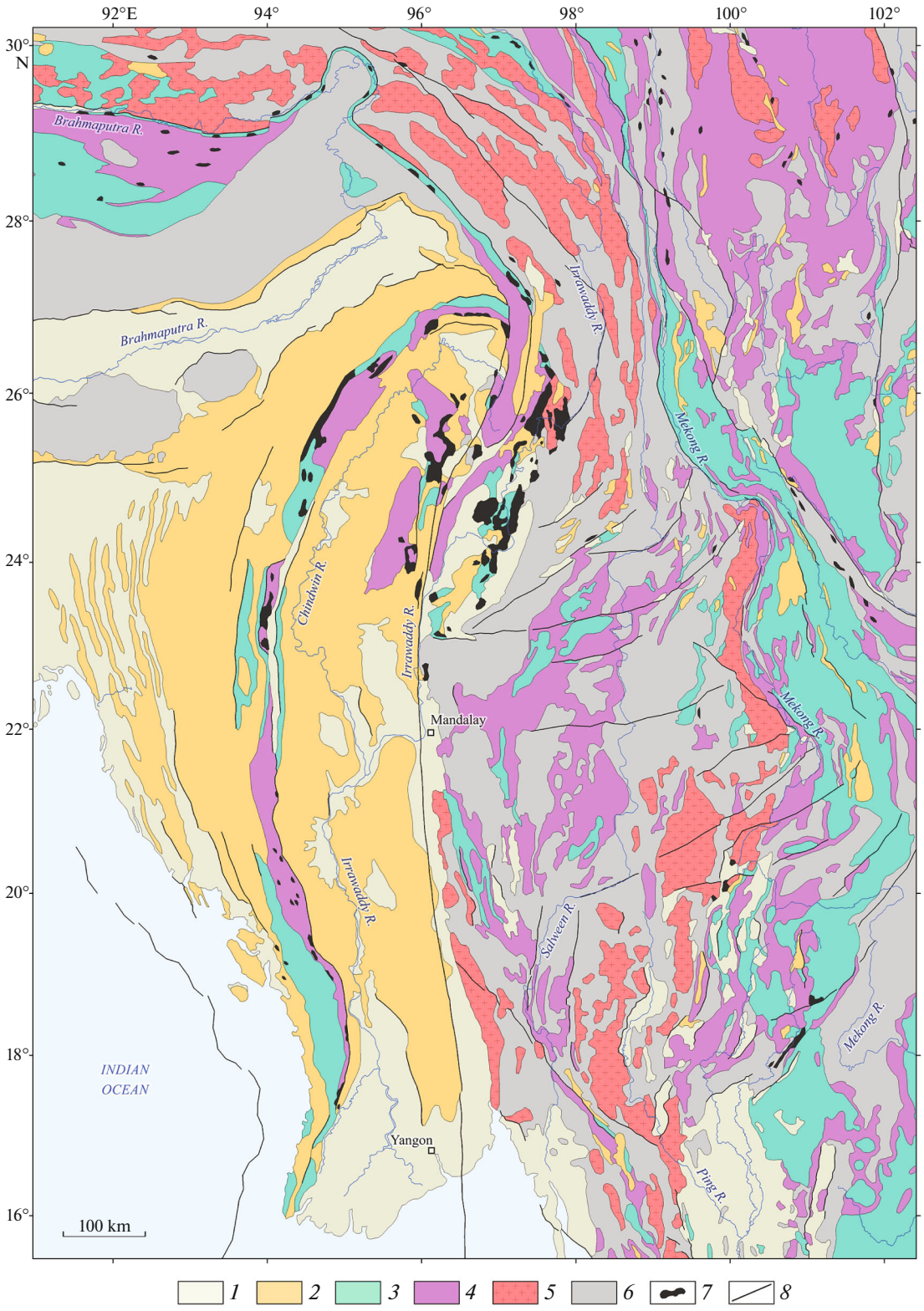

Fig. 2. Geological map of Myanmar and adjacent territories (compiled from data [28, 29, 35]). *1–4*, Sedimentary rocks: *1*, Pliocene-Quaternary; *2*, Paleogene–Neogene; *3*, Jurassic–Cretaceous; *4*, Permian–Triassic; *5*, Mesozoic granitoids; *6*, Paleozoic–Precambrian formations; *7*, ophiolites; *8*, neotectonic faults.

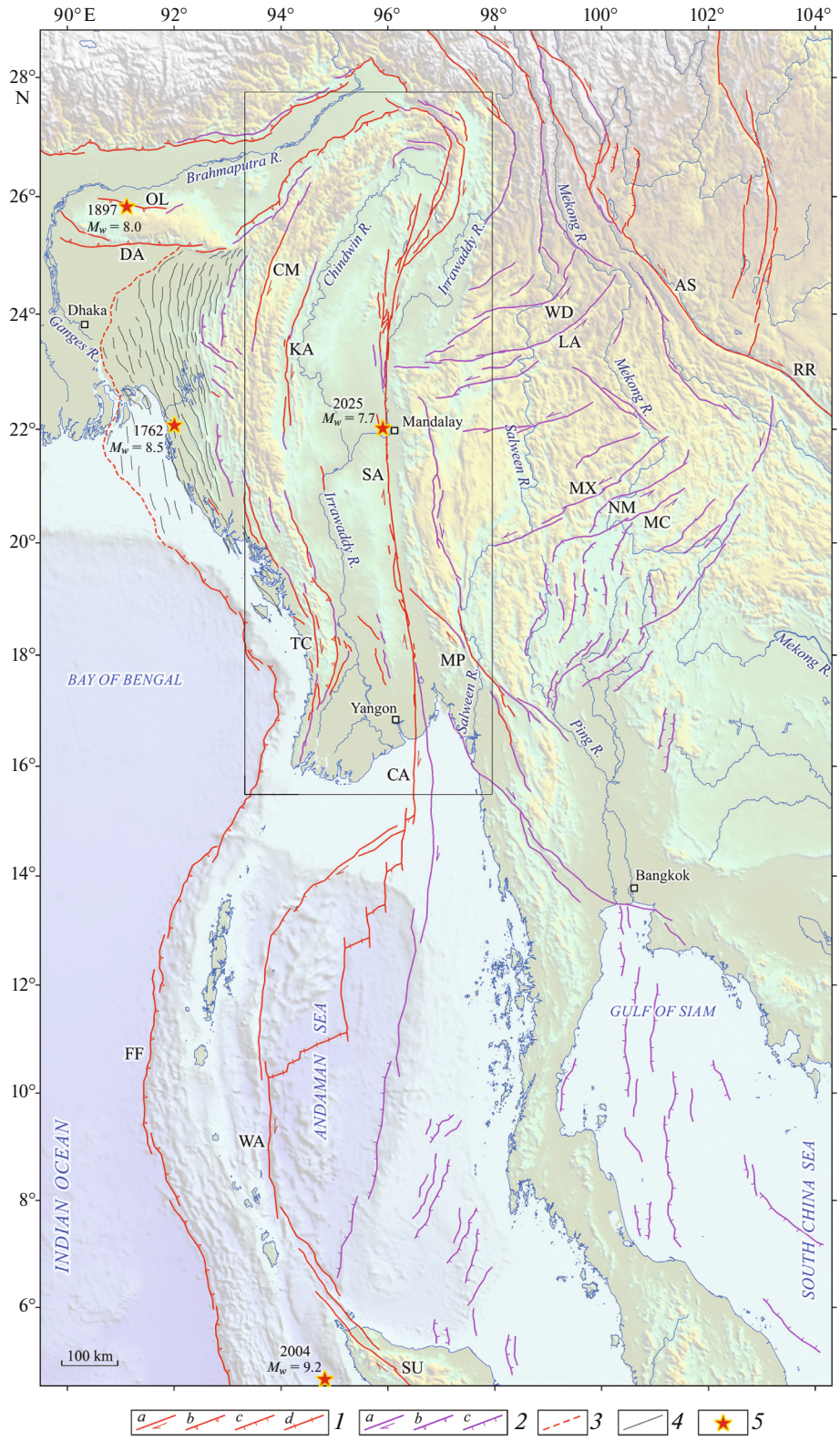

Fig. 3. Major active faults of Myanmar, Andaman Sea, and adjacent areas (compiled using data [57]). *Active Rifts*: ASH, Ayla Shan; DA, Dawkey; WA, West Andaman; KA, Kabaw; RR, Red River; ON, Oldban; SA, Sagaing; SU, Sumatran; FR, Frontal Fault of Sunda Arc; CM, Churachandpur-Mao. *Pliocene-Quaternary faults*: WO, Wonding; LA, Lakhna; MP, Mao Ping; MS, Mengxing; MC, Mae Chan; NM, Nam Ma; TC, Takhtay–Chaung. Position of Fig. 4 is shown by rectangle). *1*, Active faults: (*a*) strike-slip faults; (*b*) thrusts, (*c*) normal faults, (*d*) extension faults; *2*, Pliocene–Quaternary faults; (*a*) strike-slip faults, (*b*) thrusts, (*c*) normal faults; *3*, inferred continuation of the Frontal Rift; *4*, axes of Quaternary folds of Tripura belt; *5*, epicenters of strongest earthquakes with year and magnitude indicated.

face from the Indian Plate with thinned continental crust, which has been pushed under them. The detachment surface and underlying part of the Indian Plate form a seismic focal zone with gentle seismic slip surfaces and imbricated thrusts. Under the Tripura fold belt, the detachment surface is gently dipping to the east and at a depth of 3–5 km; under the Indo-Burmese Ranges, the dip angle of the detachment surface increases to 7° and it deepens to ~10 km [49].

Under the high eastern part of the Indo-Burmese ranges, the seismic focal zone sharply increases its angle of inclination and plunges 160 km under the Central Burmese Basin. At the same time, the crust becomes oceanic. The petrochemistry of Pliocene andesites, dacites, and rhyolites shows that they erupted from melts above a subducted slab of oceanic lithosphere [57].

Ophiolites occur among the sedimentary rocks of the Indo-Burmese Ranges and the Central Burma Trough. Hutchison [34] identified two ophiolite belts in Myanmar:

— Western (Naga Hills Line);

— Eastern (Mandalay Line).

In [33], the eastern belt is divided into two belts by the Sagaing Fault and Neogene–Quaternary sediments of the Irrawaddy River valley (Fig. 2); i.e., a total of three ophiolite belts are distinguished: the Western, Central and Eastern.

The western belt extends from northeastern India (Naga Hills) along the eastern edge of the Indo-Burmese Rang zone through all of western Myanmar to the Andaman Islands (Fig. 1). The Central and Eastern belts (Mandalay Line) are exposed only in northern Myanmar and are buried under molasses of the Central Burma Trough to the south.

The belts hosts ultramafic rocks, gabbros, mafic dikes, basalt pillow lavas, intermediate igneous rocks, and radiolarites. All three belts are petrochemically similar with some differences in ore mineralization, explained by local rock-formation features and subsequent alteration [33].

The ophiolites of the Western Belt, which corresponds to the zone of negative gravity anomalies, occur mainly as rootless subhorizontal bodies, tectonically overlapping the Eocene–Oligocene deposits [12]. Apparently, these ophiolites were obducted from the eastern belts. In the Central and Eastern belts, ophiolites often form steeply inclined bodies. The area of their distribution corresponds to a positive gravitational anomaly [12].

Compelling arguments are presented in favor of the fact that initially the ophiolites of the Central Belt were built up by ophiolites of the Eastern Belt to the north and were were displaced to their present position later by the right-lateral strike-slip fault along the Sagaing Fault in connection with the NNE drift of the Indian Plate. The right-lateral offset is estimated at 400 km [46] or 300 km since the end of the Middle Miocene [33]. Another estimate of the total displacement along the Sagaing Fault is based on the assumption that the Irrawaddy River formerly flowed along the Chinguin River valley and took its current position as a result of movements along the fault. In this case, the offset is 360 km [57].

Thus, the ophiolites of the three identified belts are deformed fragments of a single ophiolite belt of Myanmar, formed in the Mesotethys subduction zone and coinciding with the modern magmatic arc. Oceanic crust, which served as the material for the ophiolite belt, was formed in the mid-ocean ridge in the Middle Triassic–Early Jurassic, later serpentinized, subducted in the Upper Jurassic, and later underwent various degrees of metamorphism [17]. The rocks of the ophiolite complex are adjacent to Triassic–Cretaceous flysch.

The obtained datings of the oceanic crustal rocks are summarized in [33]:

— ~173 Ma, Aalenian (U–Pb determinations for gabbro and diorite from the Eastern Belt [40]);

— 160–176 Ma, Middle Jurassic (U–Pb determinations for leucogabbro from plagiogranites and andesite–basalts of the Eastern Belt [75]);

— 158 ± 20 Ma, Middle Jurassic–Valanginian (K–Ar determination for pegmatite from the hornblendite of the Western Belt [50]);

— ~127 Ma, Barremian (U–Pb determination for zircon in rodingite from serpentinite of the Western Belt [42]).

Numerous datings reflect the alterations of the Central Belt ophiolites (jadeite, blueschists, eclogite and amphibolite alterations) that occurred during the formation of the Mesotethys ophiolite belt and the subsequent overlay of the Sunda Arc magmatic belt. These dates range from 152.4 ± 1.5 Ma (Kimmeridgian) through the Aptian, Cenomanian, and Campanian to 44.8 ± 1.1 Ma (Middle Eocene). There is also evidence for later effects: ~30 Ma (Early Oligocene) and ~15 Ma (Middle Miocene) [33].

The main features of the modern structure of Myanmar began to form in the Middle Miocene. It has been established that from this time onwards there was an uplift of the Shillong Plateau and Indo-Burmese Ranges, subsidence of the Central Burma Trough, strike-slip movements along the Sagaing Fault, and, as shown below, development of the Shin Plateau faults and spreading in the Andaman Sea.

Sino-Burmese Continental Block

The main part of the block is located on the territory of Myanmar (Shin Plateau) [17, 48] (Figs. 1, 2). Its western boundary is the tectonic contact of the ophiolites of the Central Burma Trough with metamorphic rocks. The Sagaing Fault runs roughly along this boundary. The block continues north into neighboring China's Yunnan Province and east into Thai-

land. The basement of the block includes the Early Precambrian (Mogok Complex) [10, 55]. The rocks of the lower part of the complex were metamorphosed to granulite facies, and the upper part, to amphibolite facies. They are classified as Archean and/or Lower Proterozoic. The Mogok Complex is unconformably overlain by thick flyschoid strata, intensely crumpled but relatively weakly metamorphosed, spanning the Middle Proterozoic and possibly the lower parts of the Upper Proterozoic. The strata are intruded by dolerites, diorites, and granites, with datings in the range 982–834 Ma [10].

Precambrian rocks are unconformably overlain by the Upper Cambrian. From this time on, during the Paleozoic and a significant part of the Mesozoic, the Sino-Burmese block was covered by a sea in which thin carbonate–terrigenous sediments accumulated. In the center of the block, islands occasionally emerged, serving as sources of debris input. In the Late Carboniferous–Early Permian, glacial deposits accumulated, indicating that the block belonged to continental Gondwana [10]. Later, the Triassic oceanic basin, expressed by the Myanmar ophiolites, separated the Sino-Burmese block from the Hindustan part of Gondwana.

Indosinian Continental Block

The block is located on the territory of Vietnam, Cambodia, and Laos and is separated from the South China continental block by the Vietnamese fold zone, which inherited the Late Paleozoic suture (Fig. 1). The Middle Devonian volcanic belt is associated with subduction of the Vietnam oceanic trough. In the Late Devonian, folding and uplift intensified. In the Late Triassic, intense Indo-Sinian deformations took place. Along the northern edge of the fold zone runs the active Aila Shan–Red River fault system. The maximum right-lateral displacement along the Red River fault is estimated at 5.5 [14] to 40 km, of which 16 km fall on the Pliocene–Quaternary [54]. The Holocene displacement rate is ~5 mm/yr [14, 53].

In the east, the Indosinian block faces the South China Sea, and in the west and southwest, it is bounded by ophiolitic relics of the Indosinian [1], or Yunnan-Malay [10], segment of the Paleotethys. Ophiolites that formed prior to and including the Early Triassic are combined with Upper Paleozoic and Triassic strata, locally including Devonian, that deposited on the slopes of a deep-sea trough. It closed in the middle or end of the Late Triassic, when the strata experienced intense fold–thrust deformations during the Indosinian orogeny. The fold complexes are unconformably overlain by Norian–Jurassic red rocks.

The basement of the Indosinian block, similar to that of the Sino-Burmese block, outcrops in Vietnam [10]. The oldest, Kannak Complex is represented by rocks of the granulite facies of metamorphism for volcanics, and higher up, for terrigenous–carbonate rocks and granites. The complex is presumably attributed to the Archean, since the less deformed Ngoklin Complex is dated at 2.3 Ga. Early and Middle Proterozoic metasediments have been altered to amphibolite facies. They are cut through by granitoids with ages of 1.3–1.0 Ga. In the Late Proterozoic and the first half of the Paleozoic, uplifts dominated. In the Early Carboniferous, subsidence resumed. Permian magmatism is expressed by terrestrial felsic eruptions and granite formation. Uplifts and volcanism continued into the Triassic. In the Late Cretaceous, the Korat Basin formed in the north of the block, where 1.4 km of salt-bearing sediments accumulated.

Between the Sagaing right-lateral strike-slip faults and the Aila Shan–Red River system, in a triangle encompassing the Sino-Burmese block and the northern part of the Indosinian block, a series of new faults emerged in Miocene–Quaternary [57] (Fig. 3). It comprises left-lateral strike-slips with a latitudinal–northeastern strike (the Wonding, Mengxing, and Nam Ma faults), arcuate to the south. In northern Thailand, near the border with Myanmar, the Mae Chan fault (left-lateral strike-slip (?)) is distinguished. The total displacement along the left-lateral faults is estimated at 5–24 km over 5–20 Ma according to the displacements of the river valleys [38]. The system of left-lateral strike-slip faults is locally crosscut by more rectilinear right-lateral strike-slip faults with a northwestern strike (e.g., the Mao Ping fault, which is a branch of the Sagaing Fault). The neotectonic NW-trending faults continue south into Thailand.

Southern and Northern Continuations of the Tectonic Zones of Northern Indochina

The given series of tectonic zones can be traced to the south. The Indosinian block continues through the western shallow part of the South China Sea to Kalimantan Island, in the southwest of which, in the Shvaner massif, ancient crystalline schists are overlain by Upper Paleozoic shallow-water deposits of the Jurassic and Cretaceous and intruded by Upper Jurassic and Cretaceous granitoids (153–65 Ma) [10] (Fig. 1). The southern continuation of the Indosinian suture obliquely crosses the Malacca Peninsula [1]. The continuation of the Sino-Burmese block may be the eastern shelf of the Andaman back-arc sea, disturbed by a series of low-active Late Pliocene–Quaternary grabens [57].

The southern extension of the Myanmar ophiolites is buried by Cenozoic sediments of the Central Burma Trough. The location of the ophiolites can be estimated from the continuation of the right-lateral Sagaing strike-slip fault, which in the northern Andaman Sea is divided into three branches [57] (Fig. 3). Its main central branch continues to the southwest, turning into an en echelon series of southwest-trending rifts separated by two or three meridional transform

faults. The series of rifts is bounded in the southwest by the northern end of the Sumatran right-lateral strike-slip fault. The rifts form the Central Andaman Basin with a sediment thickness of ~1 km and represent a spreading center with an oceanic crust type. The spreading center opened in the middle Miocene [31]. There is an opinion about its origin ~4 Ma ago, and at first the spreading was slow, 16 mm/year, but in the last 0.7 Ma it became fast, 38 mm/year [51]. However, such a spreading rate contradicts the modern rates of displacement of ~20 mm/year along the Sagaing Fault [44, 69] and 23 mm/year along the Sumatran fault [27]. Therefore, the opinion about the origin of spreading in the Middle Miocene seems preferable.

The spreading center is bounded in the northwest by the arcuate western branch of the Sagaing Fault. In the west, it passes into the West Andaman right-lateral strike-slip fault, which continues to the southeast as the Sumatran strike-slip fault (Fig. 3). The inferred third, meridional continuation of the Sagaing Fault, as a zone of weakeness, is determined the position of the East Andaman depression, adjacent to the Sumatran strike-slip fault in the south. In the trough and on its boundaries, signs of right-lateral and extensional faulting were revealed, which caused subsidence. An additional factor in the subsidence was the isostatic reaction to accumulation of Neogene–Quaternary sediments up to 8 km thick, transported by the Irrawaddy River [57].

The continuing uncertainty of the southern continuation of the Myanmar ophiolites (Mesotethys sutures) requires consideration of the nature of the Andaman segment of the Sunda island arc. It was shown above that the northern part of the Central Burma Trough, containing products of Pliocene–Quaternary island-arc volcanism, represents the magmatic part of the modern island arc inherited from the Mesotethys, and the Indo-Burmese Ranges are an accretionary wedge before its front. Koko Island, the northernmost of the Andaman Islands have a similar structure, where seismic profiling shows that ophiolites are thrust from the east onto an accretionary wedge [57].

To the south, the structure of the arc changes. On Barren Island in the rear of the arc, plagioclase xenoliths from island-arc lava showed an $^{40}Ar/^{39}Ar$ age of 106 ± 3 Ma (Albian) [52]. Xenoliths originated from gabbro of the oceanic lower crust. The thickness of the crust, according to the seismic section, reaches continental values (24–32 km). In the southern Andaman Islands, ophiolites lie at the base [50]. Their upper mantle components—harzburgites and dunites—are overlain by a cumulative peridotite–gabbro complex, intrusive rocks of a higher crustal level, and tholeiites. The upper crust also contains significant andesitic–dacitic volcanic series, indicating island-arc volcanism on oceanic crust.

U–Pb dating of zircons from trondhjemite on the southern island yielded an age of 95 ± 2 Ma (Cenomanian) [50]. Basalt pillow lavas and dikes that cut through trondhjemite are similar in their trace element geochemistry to mid-ocean ridge rocks. The presented data show that the Andaman segment of the volcanic arc arose on the Albian–Cenomanian ophiolite-oceanic crust and is close in age to the ophiolites of the Indus–Yarlung–Tsangpo zone [13, 43]. According to [12], the ophiolites of the Andaman Islands were formed as a result of Late Oligocene collision of the Indochinese margin of Eurasia with the ensialic arc that existed within the oceanic part of the Indian Plate. Relics of this arc do not extend north into the Indo-Burmese segment of the modern Sunda Arc.

Other tectonic zones of northern Indochina also have analogues in Tibet and southern China (Fig. 1). The ophiolite belt of Myanmar is a continuation of the Bangong–Nojiang suture of Tibet [1, 2, 10, 17, 23, 33, 42]. The Indosinian suture is similar to the Jinsha suture, which hosts the Ulan-Ula and Yushu ophiolite zones; the closure of these basins began in the Late Permian and ended in the Triassic [2, 76, 77]. With such a comparison, the Sino-Burmese and Indosinian blocks correlate, respectively, with the Qiangtang and Songpan Tibet continental block. At the same time, the basement of the Sino-Burmese and Indosinian blocks has features similar to the basement of the South China block [10].

ACTIVE TECTONICS OF THE TERRITORY OF MYANMAR AND ITS SURROUNDINGS

Seismic Activity of the Indo-Burmese Ranges and Their Surroundings

During the closure of the Neotethys, the convergence rate between India and Eurasia slowed in the north from 15 to 4 cm/year [47]. The ongoing NNE movement of the Indian Plate, combined with clockwise rotation in Yunnan and Northern Myanmar, determined the modern oblique subduction of the Indian Plate under the Indo-Burmese Ranges and the Central Burma Trough with predominance of the right-lateral strike-slip component [57].

Modern tectonic activity of the plate boundary was manifested under the Sunda Arc by the powerful 2004 Sumatra–Andaman earthquake with $M_w = 9.2$, which ruptured 1300 km of the Indian Plate boundary south of Myanmar. The 1762 Arakan earthquake occurred in the northernmost Arakan segment of the Sunda Arc (southern Bangladesh) (Fig. 3). At the same time, displacement of 9–16 m could have occurred under the islands, which may indicate a magnitude of $M_w = 8.5$ [71].

During the instrumental period, the activity of the subducting Indian Plate has been expressed under the Indo-Burmese ridges as weak and rarely strong (the Tamenglang earthquake of 2016 with $M_w = 6.7$) upper crustal seismic events in the near-surface part of the Indian Plate. The *P*-axes of the focal mechanisms are oriented along the ranges, indicating dominance of

the strike-slip component [39]. This movement is transmitted to the allochthonous plate, where the rate of total modern movement is estimated at 35 mm/yr in a 10° north-northeast direction [58]. Of these, more than half are right-lateral displacements along the Sagaing Fault, which extends over the eastern margin of the steeply subducting region of the Indian Plate. The rest occurs further west, mainly in the Indo-Burmese Ranges.

In the Tripura fold belt, GPS measurements have revealed shortening at a rate of 10–13 mm/year [26, 59]. In the Naga Hills, the shortening rate is 1–4 mm/yr [68]. In the high part of the Indo-Burmese Ranges, transverse shortening, if any, is very small, but active longitudinal right-lateral strike-slip faults have been detected [72]. GPS monitoring in the area of the Churachandpur-Mao and Kabaw faults shows right-lateral displacement at a rate of up to 16 mm/year, of which the Churachandpur-Mao fault accounts for ~6 mm/year [45] (Fig. 3). On the Kabaw fault, GPS observations have established right-lateral dispalcement at a rate of 8.4 ± 3.0 mm/year with transverse shortening at a rate of 5.7 ± 4.1 mm/year [49].

On the Shillong Plateau, according to GPS data, the rate of lateral shortening is 3–6 mm/year. The rate of uplift is determined to be 0.7–1.4 mm/year in the east of the plateau, where its shortening increases to 5–7 mm/year [68]. The south-dipping hidden Oldban thrust fault on the northern boundary of the plateau is associated with the Great Assam earthquake of 1897 with a magnitude of $M_s = 8 \pm 1$ [21]. The earthquake caused a displacement of 25 ± 5 m. A thick (up to 35 km) seismogenic layer spanned the entire crust, which indicates its relationship with the Indian Platform.

Sagaing Fault

The meridional active right-lateral Sagaing strike-slip fault extends across Myanmar for more than 1500 km (Fig. 4). The fault is clearly visible on the ground and in satellite images. There are no significant curvatures of its line that could cause the formation of fault uplifts and depressions. In the north, the fault splits into several branches that transpressively separate the uplifts of ridges composed of metamorphic complexes. In the south, the fault continues into the Andaman Sea, where it is associated with the modern spreading center (Fig. 3).

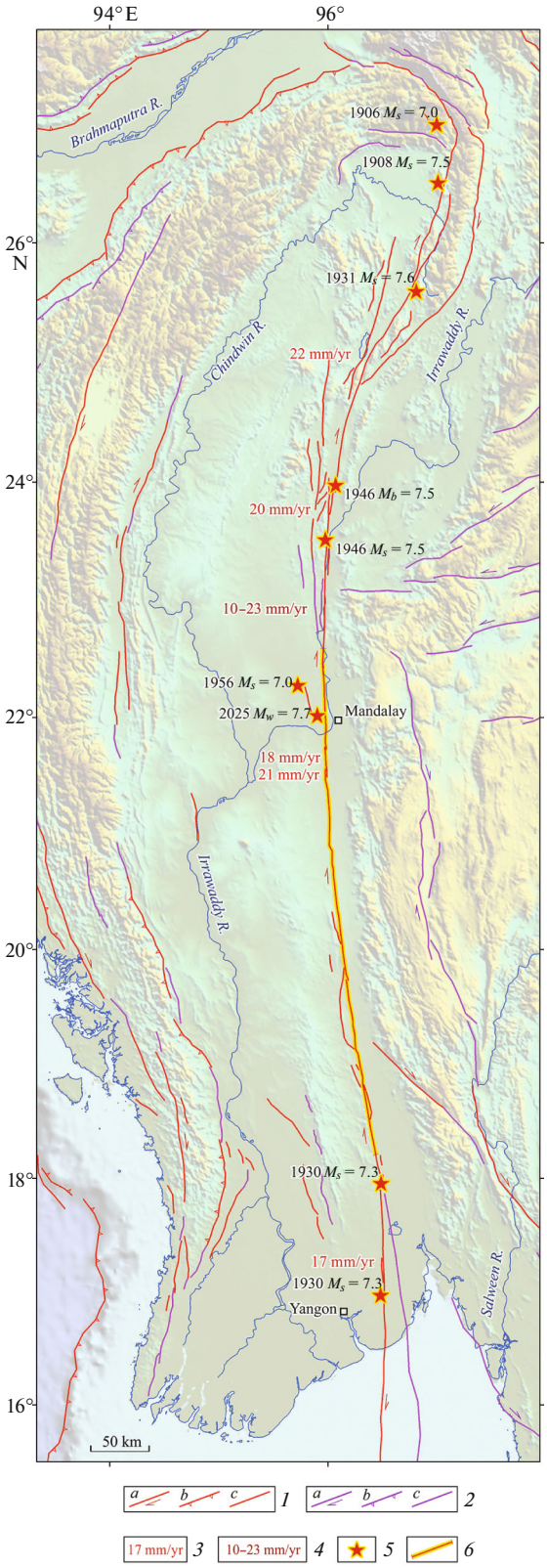

Fig. 4. Data on current activity of Sagaing Fault (according to [57], modified). *1*, Active faults: (*a*) strike-slip, (*b*) thrust, (*c*) sense unknown; *2*, Pliocene–Quaternary faults; (*a*) strike-slip, (*b*) thrust, (*c*) sense unknown; *3*, displacement rates based on GPS monitoring results; *4*, displacement rates based on geological observations; *5*, epicenters of earthquakes with magnitudes of at least $M \geq 7$ associated with Sagaing Fault (years and magnitudes M_w, M_b or M_s are given); *6*, Sagaing Fault segment activated by 2025 Mandalay earthquake.

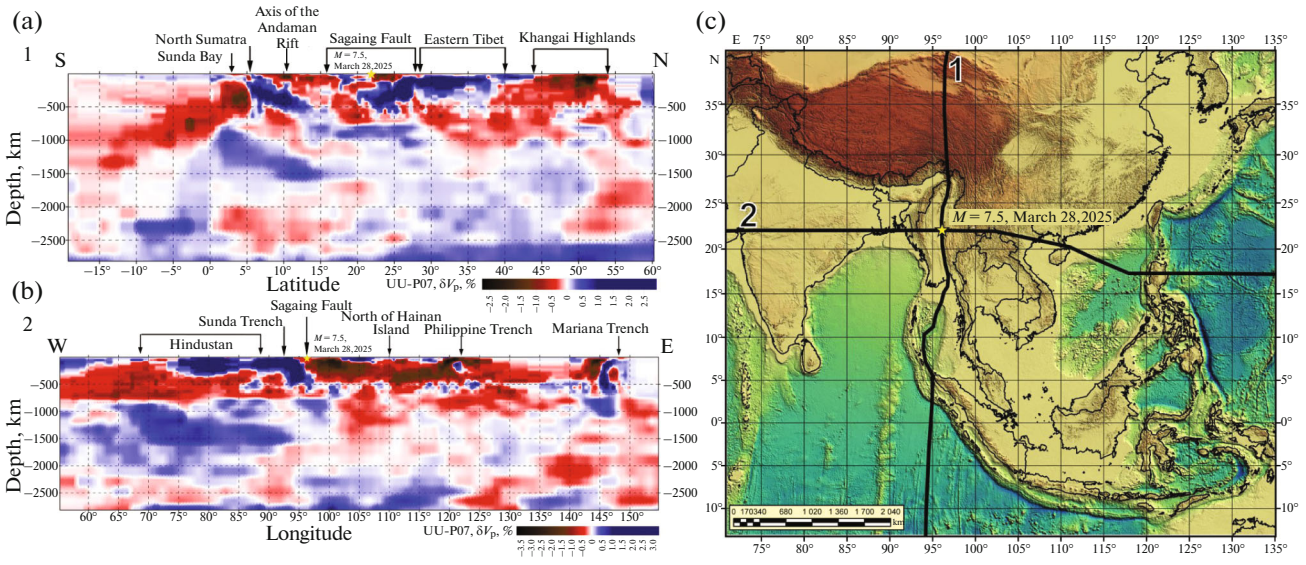

Fig. 5. Seismic tomography sections of UU-P07 volumetric model of *P*-wave velocity variations through Myanmar–Yunnan intramantle plume in Southeast Asia (based on [9, 11, 63]). Yellow star shows position of epicenter of Mandalay event $M = 7.5$ (March 28, 2025). (a) Submeridional seismic tomography section 1; (b) sublatitudinal seismic tomography section 2; (c) position of seismic tomography sections: 1, submeridional; 2, sublatitudinal.

GPS monitoring data showed that in the northern part of the fault, for 400 km north of Mandalay, the strike-slip rates consistently range from 18 to 22 mm/year [44, 69]. In the south, the rate was determined to be 17 mm/year. In the south of the fault, displacement of the walls of a 16th century fort has been described, which determines the shear rate of 11–18 mm/year [73]. Further north, displacement of a lava flow with a K–Ar age of 0.25–0.3 Ma has been identified, yielding a shear rate of 10–23 mm/yr [20].

Sources of instrumental earthquakes with $M \geq 7$ were distributed along the Sagaing Fault as follows [57] (Fig. 4):

— In 1930, two earthquakes with $M_w = 7.3$ occurred in the south of the fault with the formation of a seismogenic rupture 120 km long with a displacement of >3 m [64];

— in 1931, an earthquake with $M_s = 7.6$ occurred at the northern end of the fault;

— sources of two earthquakes with $M_b = 7.5$ and $M_s = 7.8$, which occurred in 1946, were successively located south of the 1931 earthquake; in 1991, 1992, and 2012, three earthquakes with $M_w > 6$ occurred in the same area;

— in 1956, further south, but north of Mandalay, an earthquake with $M_s = 7.0$ occurred.

In [72], this successive migration of seismic events was noted and the possibility of an earthquake with $M_w = 7.8–7.9$ was predicted on the fault segment between the 1956 and 1930 earthquakes.

The 2025 Mandalay earthquake occurred on this segment of the fault, and the resulting seismic rupture zone closed the interval (Fig. 4). Approximately at the site of the 2025 seismic rupture, 184 years earlier, the strongest earthquake occurred in 1839 [39]. This gives an idea of the possible recurrence interval of earthquakes with magnitudes of at least $M \geq 7$ in the Sagaing Fault Zone.

DEEP STRUCTURE OF INDOCHINA BASED ON SEISMIC TOMOGRAPHY DATA

The deep structure of Indochina was determined based on seismic tomography data. Submeridional section 1 (Fig. 5), calculated along the Sagaing strike-slip fault, shows the presence of an upper mantle plume along it, which in the plane of the section rises from a depth of ~700 km and expands towards the surface to the north and south, covering the "cold" volumes of the mantle and demonstrating, thus, the contrast of the rheological state of the mantle. To the north of this region, an intramantle plume is observed, rising from a depth of ~1500 km and spreading to the surface under Central Tibet (outside the plane of the section) and the Khangai Plateau.

South of the Sagaing Fault, a contrasting state of the mantle is also observed due to the presence of a slab under the Sunda Arc, which flattens out under the root of the upper mantle plume at a latitude of ~17° N. South of the Sunda Arc, the branches of the African and Pacific superplumes probably overlap, which in the Northeast Indian Ocean merge into a single hot volume [5] with the predominance, most likely, of material from the Pacific plume. The greatest contrast in the rheological state of the mantle, in which the most mobile (hot) and cold volumes of the mantle interact, is expressed in the central part of the Sagaing

Fault. In this geodynamic setting, significant stresses are expected to accumulate in the transition zone between mantle volumes of different rheology and be released in the form of strong seismic events.

Sublatitudinal section 2 (Fig. 5), calculated across the Sagaing Fault from the epicenter of the Mandalay earthquake, shows the presence of a sharp contrast in δVp on flanks of the fault plane. To the west of the epicenter in the upper mantle is the "cold" Hindustan lithospheric block, and to the east is the "hot" mobile block of the Indochina Peninsula, in which the movement of lithospheric masses to the south is clearly evident, recorded by GPS data [61, 70] and forming the displacement kinematics. This "hot" anomaly extends eastward to the eastern border of the Philippines, after which the structure of the upper mantle changes. Within the specified segment, plumes with mid-mantle roots are distinguished, and in the easternmost part of the segment, "hot" anomalies of the Pacific superplume with roots at the mantle–core boundary are visible [6].

Sublatitudinal section 2 (Fig. 5) also shows horizontal stratification of the mantle both in "hot" and "cold" volumes. The most contrast in terms of δVp of segment 2 corresponds to the Sagaing right-lateral strike-slip fault, which in the south, near 10° N, forms the rift segment of the Andaman Sea, the intense seismicity of which in the west coincides with the epicenters of the Sunda Arc.

SEISMOTECTONIC MANIFESTATIONS OF THE MANDALAY EARTHQUAKE

Seismotectonic interpretation of remote sensing data relies on primary seismological data [66]. The solution of the earthquake source corresponds to a strike-slip mechanism with vertical nodal planes having an azimuth of 270° (left-lateral strike-slip) and 1° (right-lateral strike-slip). The focal zone, determined by the distribution of aftershocks, is strictly confined to the Sagaing Fault and has a general north–south trend. Eyewitness accounts confirm the right-lateral shear kinematics of movement without a significant vertical component [22].

The actual position of the seismic rupture zone was mapped from an interferogram calculated from Sentinel-1 radar images before and after the earthquake (Fig. 6).

It was found that the rupture line is almost straight and is located entirely on the previously mapped Sagaing Fault line [57]. At the northern end of the seismic ruptures, compensatory extension structures have developed, which are shown in remote sensing data as subsidence surfaces in the eastern limb of the fault. To the south of the seismic rupture zone, for 180 km up to the coastline, a slip of the same sense, but no more than 20 cm in amplitude, can be traced in the interference pattern. Since seismic events were not recorded in this area, this displacement is apparently creep.

The rupture in the earthquake's source reached the surface over a distance of 460 km. The displacement values range from 0 m at the edges of the rupture to 4.2 m according to interferometry data or up to 5.8 m according to optical image correlation (Fig. 6). In the zone of maximum displacements, the interferometry data are underestimated due to insufficient spatial resolution. However, even for optical survey data, the displacement is averaged over a window of about 100 m; i.e., the maximum displacement measured on the ground may be even greater. Similar, though less detailed displacement data have been published by NASA's Operational Monitoring Services [16] and the Japan Aerospace Exploration Agency [25], which confirms the obtained estimates.

DISCUSSION

Characteristic Features of the Mandalay Earthquake and Comparison with the Strongest Earthquakes in Eastern Anatolia

The Mandalay Earthquake of March 28, 2025, with a magnitude $M_w = 7.7$ is characterized by the following features.

— The earthquake's source is located in a zone of a large and extended active right-lateral strike-slip fault in the upper part of the crust. During the earthquake, right-lateral displacement occurred along this fault.

— The seismogenic rupture zone that emerged during the earthquake and represented the intersection of the source with the Earth's surface has a length of 460 km, which is anomalously large for the given magnitude (Fig. 7). In this case, the earthquake's source does not extend beyond the upper part of the crust. The depth of the hypocenter is ~10 km.

— The fault is located in an ophiolite substrate, which facilitates rock slip.

— The fault zone and earthquake source are located above a mantle plume, which has reduced the thickness of the mantle portion of the lithosphere and caused softening of the lower part of the crust.

The above features of the Mandalay earthquake show similarities with the three strongest earthquakes in Eastern Anatolia that have occurred in the last 80 years (Fig. 8):

— the Erzincan earthquake of November 26, 1939 (23:57 UTC);

— the East Anatolian (Pazarcik) earthquake of Februry 6, 2023 (01:17 UTC);

— the Elbistan earthquake Februry 6, 2023 (10:24 UTC).

The magnitude of the Erzincan earthquake is estimated at $M_w = 7.8$ [36]. The earthquake created a 360-km-long seismic rupture zone along the North Anatolian right-lateral fault zone. Along the seismic faults, right-lateral displacement occurred with an average amplitude of 3.7 m and up to 7–8 m near the

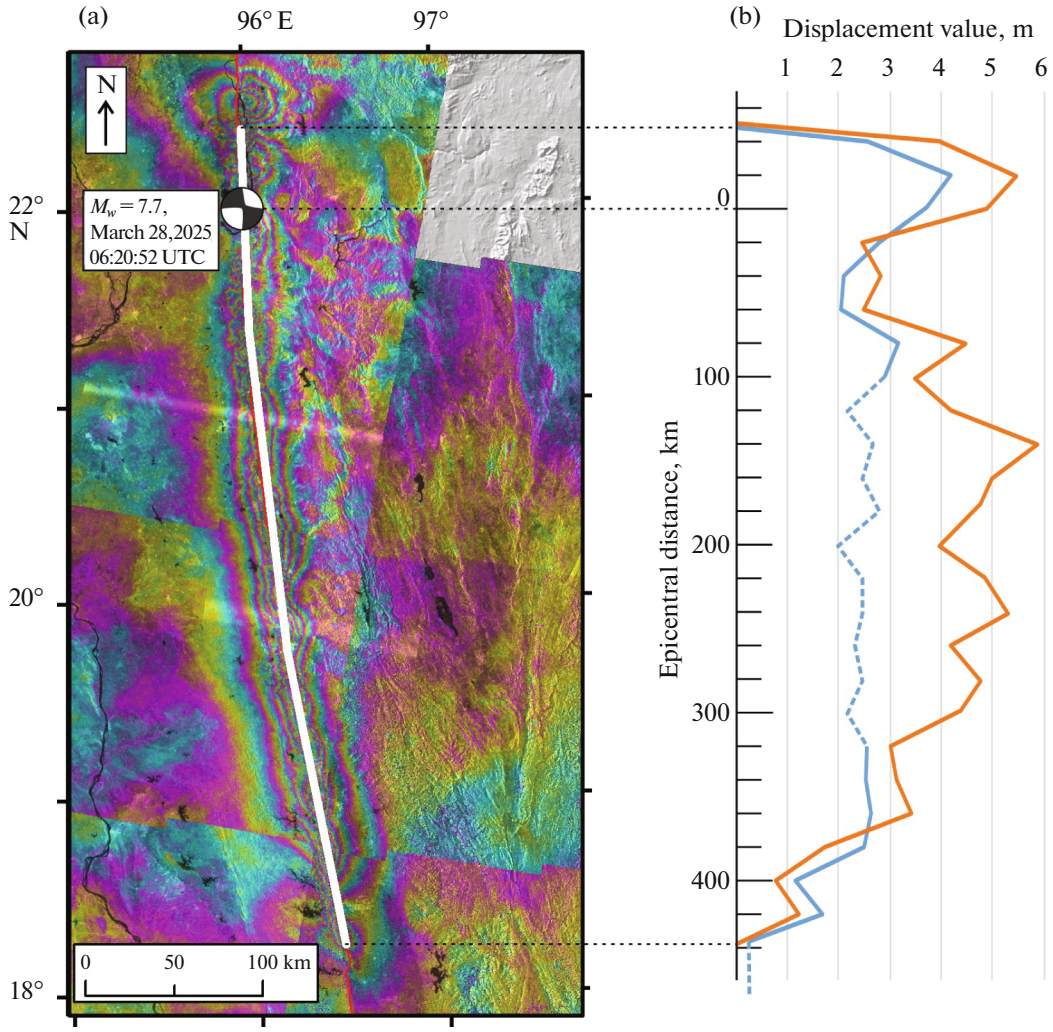

Fig. 6. Seismotectonic data obtained on Mandalay earthquake. (a) Position of seismic rupture (white line) on interferogram obtained from Sentinel-1 images (according to [62]); (b) displacement amplitudes along fault according to radar survey data (blue line) and optical images (orange line).

epicenter, where the variable vertical displacement component reached 2 m [18, 63]. The epicenter was located near the city of Erzincan; the depth of the hypocenter was ~20 km.

During the East Anatolian (Pazarcik) earthquake (M_w = 7.7–7.8 [37, 65]) along the East Anatolian left-lateral strike-slip fault zone, a 361-km-long seismic fault zone emerged [11]. The seismic faults also covered the western and eastern branches of the left-lateral Dead Sea Transform Fault, adjacent to the East Anatolian zone from the south, over a length of 16 and 41 km, respectively. Along seismic faults over a distance of 318 km, left-lateral displacement of up to 8.5 m occurred [11].

The mentioned displacement amplitudes during the earthquakes of February 6, 2023, were established by field observations of the displacements of natural and man-made objects on the Earth's surface. These amplitudes are close to the strike-slip displacement estimates based on radar satellite interferometry and seismology data [4, 24, 65]. According to interferometry data [4], during the Pazarcik earthquake, the displacement exceeded 5 m on the Earth's surface and, according to the calculated model, could have reached 12.7 m at depth. During the Elbistan earthquake, the displacement exceeded 7 m on the surface and, according to the calculated model, could have reached 10 m at depth [4].

During the Elbistan earthquake (M_w = 7.5–7.6 [37, 65]) along the active Chardak and Uluova faults with a dominant left-lateral displacement component, a seismic rupture zone with a length of 190 km emerged; along the seismic ruptures, left-lateral displacement with an amplitude of up to 7.84 m was recorded over a length of 148 km [9].

Given the significant length of the seismic rupture zones, the depths of the hypocenters of both earthquakes on February 6, 2023, are close to 10 km, and the depths of hypocenters of the strongest aftershocks do not exceed 18–20 km [37, 65]. Thus, the focal

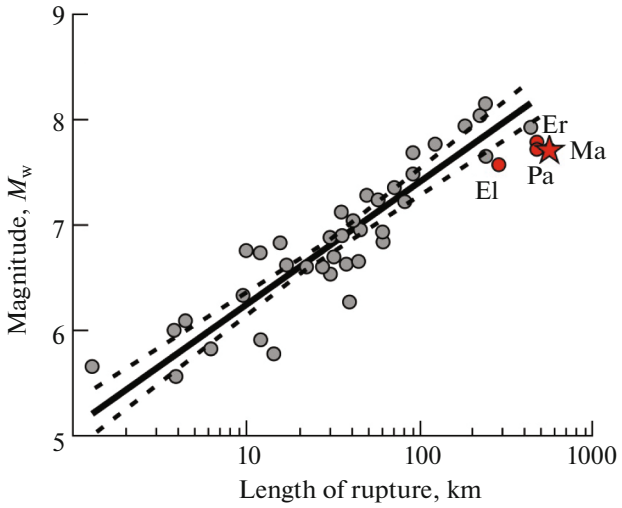

Fig. 7. Comparison of parameters of Mandalay earthquake and Erzincan, Pazardzhik, and Elbistan earthquakes with global intracrustal earthquake statistics (according to [74]). Shown: ratios of magnitude M_w and length of seismic rupture zone L for individual earthquakes (gray circles); average statistical curve of M_w and L ratios (solid line); boundaries of acceptable deviations from average curve (dotted line). M_w and L ratios for earthquakes are highlighted in red: Ma, Mandalay; Pa, Pazarcik; El, Elbistan; Er, Erzincan.

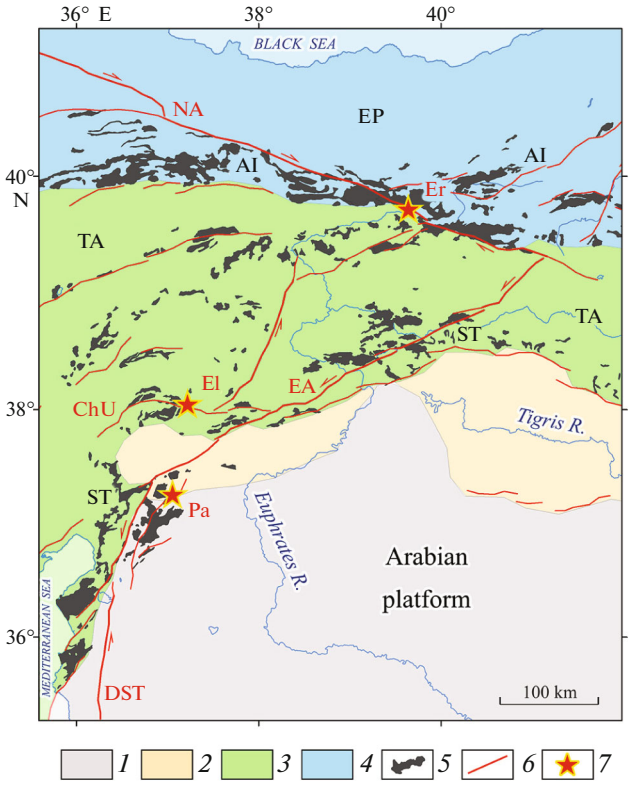

Fig. 8. Tectonic zones and epicenters of strongest earthquakes in Eastern Anatolia (according to [8, 9, 11, 36]). Tectonic zones: EP, Eastern Pontides (eastern part of Sakarya zone); TA, Taurides. *Sutures*: AI, Izmir–Ankara–Erzincan; ST, South Taurus. *Active Rifts*: EA, East Anatolian zone; NA, North Anatolian zone; DST, Dead Sea Transform; ChU, Chardak-Uluova. *Epicenters of earthquakes*: Er, Erzincan; El, Elbistan; Pa, Pazarcik. *1*, Weakly deformed areas of Arabian Platform; *2*, areas of Late Cenozoic deformations of Arabian Platform cover; *3–4*, zones of sutures and active margins: *3*, Neotethys; *4*, Mesotethys; *5*, ophiolite outcrops; *6*, active faults; *7*, epicenters of strongest earthquakes.

zones of both earthquakes do not extend deeper than the upper part of the crust.

All three seismic events in Eastern Anatolia are confined to zones of major strike-slip faults that have been active since the Pliocene. The resulting seismic faults represent outcrops of focal zones on the Earth's surface. The length of seismic rupture zones exceeds the permissible deviations from the average statistical values established in [74] for continental strike-slip earthquakes (Fig. 7).

Over a significant distance, seismic faults disrupt the ophiolite substrate. In the North Anatolian fault zone, the largest ophiolite fields with serpentinized peridotite bodies coincide with the intersection of the North Anatolian zone and ophiolite suture of the Izmir–Ankara–Erzincan–Sevan Mesotethys [8] (Fig. 8). The epicenter of the 1939 earthquake is in the Erzincan depression, which is the center of this intersection. The ophiolites extend along the fault zone to the northwest, where they are possibly complemented by the Paleotethys ophiolites [56]. Precisely to the northwest, in the ophiolites, the seismogenic movement of the 1939 seismic event mainly propagated.

The Chardak, Uluova, and East Anatolian fault zones, activated on February 6, 2023, except for its segment that ruptured the Arabian Plate, are located on the ophiolite substrate of the Neotethys subduction zone, which in this area dips gently and does not extend beyond the crust [9]. Fragments of the upper part of the continental crust of the Taurides lie on the ophiolites. In the focal zone of the 2023 Elbistan earthquake, it was established that in the segments where seismic ruptures intersect or bound the outcrops of ophiolites, the seismic shear displacement amplitudes are significantly higher than in neighboring segments composed of rocks of the continental crust of the Taurides or its sedimentary cover [9].

A volume of rocks with reduced *P*-wave velocities has been identified beneath Eastern Turkey and Armenia, extending from the African superplume at the level of the upper mantle and tops of the lower mantle [7]. Under the focal zones of the considered earthquakes, the roof of the rock volume with *P*-wave velocities reduced by at least 37% is located no deeper than 30 km [9]. This indicates that not only the upper mantle, but also the lower part of the crust here experiences increased heating and decompaction. We propose that the softening of the lower crust and upper mantle of Eastern Anatolia limits the seismogenic layer of the region to the upper crust. At the same time, the thermal impact of low-velocity volumes on the seismo-

genic layer reduces its viscosity, leading to an increase in the amplitudes of seismogenic movements.

The Mandalay earthquake of March 28, 2025, is similar to the East Anatolian earthquakes considered above in that it is confined to large active strike-slip faults, has a strike-slip type of seismogenic movements, has an increased length of earthquake sources expressed by seismic rupture zones, and has a shallow focal depth (10–20 km). The sources of all these earthquakes are located on an ophiolite substrate, and beneath them, the lower part of the crust and the remaining part of the lithospheric mantle are softened by the influence of the underlying low-velocity mantle.

Serpentine is formed by the interaction of olivine and enstatite, contained in peridotite, with water and contains a hydroxyl group. At the same time, in the process of serpentinization, the fayalite part of olivine can release molecular hydrogen as a result of the oxidation of divalent iron to trivalent iron. The presence of water and hydrogen increases the ability of serpentinite to deform under upper crustal conditions.

We believe that it was the presence of a ductile ophiolite substrate containing water and molecular hydrogen, and the softening of the lower crust and upper mantle, that caused the increased extent of seismic rupture zones with shallow sources that did not extend beyond the upper part of the crust. At the same time, serpentinization of peridotite increased stresses in the seismogenic volume due to decompression from 3.2 g/cm^3 in peridotite up to 2.2–2.9 g/cm^3 in serpentinite [3]. The similarity of the seismotectonic features of the Mandalay earthquake and distant earthquakes of Eastern Turkey, and, above all, the increased length of the seismic rupture zones, indicate the universality of the seismogenesis factors that caused them. These factors should be taken into account when assessing the seismic impacts of strong earthquakes.

CONCLUSIONS

1. The Mandalay Earthquake of March 28, 2025, with magnitude $M_w = 7.7$ occurred in the meridionally extending active right-lateral strike-slip Sagaing Fault Zone in Myanmar. The epicenter of the earthquake is near the city of Mandalay. The depth of the hypocenter is about 10 km.

2. The Sagaing fault is located in the east of the Central Burma Trough tectonic zone, where ophiolites are common, which are relics of the Mesotethys paleocean that formed in the Triassic or possibly Late Permian and closed in the mid-Cretaceous. In the region's neotectonic structure, the Central Burma Trough zone functions as the volcanic portion of the northernmost segment of the Sunda island arc. The Indo-Burmese Range zone to the west is the outer part of the arc—a deformed accretionary wedge under which the Indian Plate is gently subducting. At the latitude of Myanmar, the plate has thinned continental crust, which may be replaced by oceanic crust in the eastern Indo-Burmese Ranges, where the underthrust surface is sharply subsiding. The Sagaing Fault is located above the eastern flank of the steeply dipping plate. Further east are the Sino-Burmese and Indosinian continental blocks, separated by the Paleotethys suture.

3. Beneath Myanmar and the more eastern regions of northern Indochina lies the Myanmar–Yunnan mantle plume, a volume of low-velocity mantle that rises from the lower transition layer or upper lower mantle. The heated and decompressed plume rocks partially replace the lithospheric mantle and soften its relics and the lower part of the crust, limiting the seismogenic layer of the Mandalay earthquake zone to the upper part of the crust.

4. The authors processed remote sensing data before and after the Mandalay earthquake using radar interferometry and subpixel correlation of optical satellite images. The processing results showed that during the earthquake, a seismic rupture zone with a length of ~460 km emerged at the Sagaing Fault, along which right-lateral displacement with an amplitude of up to 5.8 m occurred. The displacement spread mainly to the south of the epicenter—to the segment of the Sagaing Fault unaffected by the previous strongest ($M_w \geq 7$) earthquakes of the instrumental period. The results obtained are confirmed by seismological data.

5. The length of the seismic rupture zones of the Mandalay earthquake and the three strongest earthquakes in Eastern Anatolia comparable to it is anomalously large for the corresponding magnitudes compared to the average statistical values of this magnitude. The increased length of seismic rupture zones corresponding to the focal zones of these earthquakes is due to the fact that they emerged on a ductile ophiolite substrate; the shallow depth of the sources (upper part of the crust) is associated with softening of the lower part of the crust and upper mantle under the influence of the heated and decompressed mantle volumes located below. These factors should be taken into account when predicting the seismic impacts of strong earthquakes.

ACKNOWLEDGMENTS

The authors are grateful to the reviewers A.F. Emanov (Altai–Sayan Branch, Federal Research Center Geophysical Survey, Russian Academy of Sciences (ASB FRC GS RAS), Novosibirsk, Russia), Yu.L. Rebetsky (Schmidt Institute of Physics of the Earth (IPE RAS), Moscow, Russia), and L.V. Eppelbaum (Tel Aviv University, Tel Aviv, Israel) for useful comments, as well as to M.N. Shoupletsova (Geological Institute, Russian Academy of Sciences (GIN RAS), Moscow, Russia) for careful editing.

FUNDING

The article was prepared under topics FMMG-2023-0006 and FMMG-2023-0005 of the Geological Institute, Russian Academy of Sciences.

CONFLICT OF INTEREST

The authors of this work declare that they have no conflicts of interest.

REFERENCES

1. A. A. Belov, Yu. G. Gatinsky, and A. A. Mossakovsky, "Indosinides of Eurasia," Geotectonics, No. 6, 21–42 (1985).
2. V. S. Burtman, "Tien Shan and High Asia: Tectonics and geodynamics in the Paleozoic," in *Transactions of Geological Institute of Russian Academy of Sciences*, Ed. by A. A. Mossakovsky (Moscow, GEOS, 2006) [in Russian].
3. T. P. Ivanova and V. G. Trifonov, "New aspects of the relationship between tectonics and seismicity," Dokl. Akad. Nauk **331** (5), 587–589 (1993).
4. V. O. Mikhailov, I. P. Babayantz, M. S. Volkova, E. P. Timoshkina, V. B. Smirnov, and S. A. Tikhotskii, "Earthquakes in Turkey: A model of the rupture surface based on satellite radar interferometry," Dokl. Earth Sci. **511** (1), 71–77 (2023). https://doi.org/10.31857/S2686739723600625
5. S. Yu. Sokolov, "The state of geodynamic mobility in the mantle from seismic tomography data and ratio between *P*- and *S*-wave velocities," Vestn. KRAUNTs. Nauki Zemle **24** (2), 55–67 (2014).
6. S. Yu. Sokolov and V. G. Trifonov, "Arc tectonic elements and upper mantle structure of Central and Southeast Asia: Seismic tomography and seismicity data," Geotectonics **58**, 23–40 (2024). https://doi.org/10.31857/S0016853X24010023
7. V. G. Trifonov and S. Yu. Sokolov, "Sublithospheric flows in the mantle," Geotectonics **51**, 535–548 (2017). https://doi.org/10.7868/S0016853X1706008X
8. V. G. Trifonov, S. Yu. Sokolov, S. A. Sokolov, and K. Hessami, "Mesozoic–Cenozoic structure of the Black Sea–Caucasus–Caspian Region and its relationships with the upper mantle structure," Geotectonics, No. 3, 55–81 (2020). https://doi.org/10.31857/S0016853X20030108
9. Ya. I. Trikhunkov, H. Çelik, V. S. Lomov, V. G. Trifonov, D. M. Bachmanov, Y. Karginoglu, and S. Yu. Sokolov, "Geological position, structural manifestations of the Elbistan earthquake and tectonic comparison of two strongest 06.02.2023 seismic events in Eastern Turkiye," Geotectonics **58** (3), 368–383 (2024). https://doi.org/10.31857/S0016853X24030054
10. V. E. Khain, *Tectonics of Continents and Oceans* (Nauchn. Mir, Moscow, 2001).
11. H. Çelik, Ya. I. Trikhunkov, S. A. Sokolov, V. G. Trifonov, E. A. Zelenin, Yu. Kargınoğlu, K. I. Yushin, V. S. Lomov, and D. M. Bachmanov, "Tectonic aspects of the East Anatolian 06.02.2023 Earthquake in Turkiye," Izv., Phys. Solid Earth **59**, 822–838 (2023). https://doi.org/10.31857/S0002333723060054
12. S. K. Acharyya, "Collisional emplacement history of the Naga-Andaman ophiolites and the position of the eastern Indian suture," J. Asian Earth Sci. **29** (2–3), 229–242 (2007). https://doi.org/10.1016/j.jseaes.2006.03.003
13. J. C. Aitchison, A. M. Davis, A. V. Abrajevitch, J. R. Ali, Badengzhu, J. Liu, H. Luo, I. R. C. McDermid, and S. V. Ziabrev, "Stratigraphic and sedimentological constraints on the age and tectonic evolution of the Neotethys ophiolites along the Yarlung–Tsangpo suture zone, Tibet", in *Ophiolites in Earth History*, Ed. by Y. Dilek and P. T. Robinson (*Spec. Publ.—Geol. Soc. London*, 2003, Vol. 218), pp. 147–164. https://doi.org/10.1144/GSL.SP.2003.218.01.09
14. C. R. Allen, A. R. Gillespie, Yu. Han, K. E. Sieh, B. Zhang, and Ch. Zhu, "Red River and associated faults, Yunnan Province, China: Quaternary geology, slip rates, and seismic hazard," GSA Bull. **95** (6), 686–700 (1984). https://doi.org/10.1130/0016-7606(1984)95<686:RRA-AFY>2.0.CO;2
15. M. Amaru, *Global Travel Time Tomography with 3D Reference Models, PhD Thesis* (Geol. Departm., Utrecht Univ., Germany, 2007).
16. ARIA Advanced Rapid Imaging and Analysis. https://aria.jpl.nasa.gov/ (Accessed June 16, 2025).
17. A. J. Barber, Khin Zaw, and M. J. Crow, "The pre-Cenozoic tectonic evolution of Myanmar," in *Myanmar: Geology, Resources and Tectonics,* Ed. by A. J. Barber, Khin Zao, and M. J. Crow (Geol. Soc. London, Mem., 2017, Vol. 48), pp. 687–712. https://doi.org/10.1144/M48.31
18. A. A. Barka, "The North Anatolian fault zone," Ann. Tecton. **6**, 164–195 (1992).
19. T. W. Becker and L. Boschi, "A comparison of tomographic and geodynamic mantle models," Geochem., Geophys., Geosyst. **3**, 1–48 (2002). https://doi.org/10.129/2001GC000168
20. G. Bertrand, C. Rangin, R. C. Maury, H. M. Htun, H. Bellon, and J. P. Guillaud, "Les basaltes de Singu (Myanmar): Nouvelles contraintes sur le taux de décrochement récent de la faille de Sagaing," C. R. Acad. Sci. (Ser. IIA-Earth Planet. Sci.) **327**, 479–484 (1998).
21. R. Bilham and P. England, "Plateau 'pop-up' in the great 1897 Assam earthquake," Nature **410**, 806–809 (2001).
22. K. Bradley and J. Hubbard, Remarkable video captures fault slip in the Myanmar earthquake. Earthquake Insights. https://doi.org/ html (Accessed June 16, 2025). https://doi.org/10.62481/01cd039c
23. B. C. Burchfiel and Z. Chen, *Tectonics of the Southeastern Tibetan Plateau and Its Adjacent Foreland* (GSA, Boulder, USA, GSA Mem., Vol. 210, 2012).
24. K. Ö. Çetin, J. D. Bray, J. D. Frost, A. Hortacsu, E. Miranda, R. E. S. Moss, and J. P. Stewart, *February 6, 2023 Kahramanmaras, Türkiye Earthquakes. Report on Geoscience and Engineering Impacts*, GEER Assoc. Rep. 082 ed., May 6, 2023. https://doi.org/doi:10.18118/G6PM34
25. Earthquake in Mandalay, Myanmar on 28 March, 2025. Emergency Obs. Request Information. https://sentinel-asia.org/EO/2025/article20250328MM.html (Accessed June 16, 2025).
26. V. K. Gahalaut, B. Kundu, S. S. Laishram, J. Catherine, A. Kumar, M. D. Singh, and M. Narsaiah, "Aseismic plate boundary in the Indo-Burmese wedge, northwest Sunda Arc," Geology **41** (2), 235–238 (2013). https://doi.org/10.1130/G33771.1
27. J. F. Genrich, Y. Bock, R. Mccaffrey, and L. Prawirodirdjo, "Distribution of slip at the northern Sumatran fault system," J. Geophys. Res.: Solid Earth **105**, 28327–28341 (2000). https://doi.org/10.1029/2000JB900158

28. *Geological Map of the People's Republic of China. Scale 1 : 2500000*, Ed. by Huang Chongke (Xi'an Mapp. Print. Comp. ARSC, China Geol. Surv., 2004).
29. *Geological Map of Myanmar. Scale 1 : 2250000* (Myanmar Geosci. Soc., Yangon, Myanmar, 2014).
30. R. M. Goldstein and C. Werner, "Radar interferogram filtering for geophysical applications," Geophys. Rev. Lett. **25** (21), 4035–4038 (1998). https://doi.org/10.1029/1998GL900033
31. R. Hall, "Cenozoic geological and plate tectonic evolution of SE Asia and the SW Pacific: Computer-based reconstructions, model and animations," J. Asian Earth Sci. **20**, 353–431 (2002). https://doi.org/10.1016/S1367-9120(01)00069-4
32. R. Hall and W. Spakman, "Mantle structure and tectonic history of SE Asia," Tectonophysics **658**, 14–45 (2015). https://doi.org/10.1016/j.tecto.2015.07.003
33. Hla Htay, Khin Zaw, and Than Oo, "The mafic–ultramafic (ophiolitic) rocks of Myanmar, in *Myanmar: Geology, Resources and Tectonics,* Ed. by A. J. Barber, Khin Zao, and M. J. Crow (Geol. Soc. London, Mem., 2017, Vol. 48), pp. 117–141. https://doi.org/10.1144/M48.6
34. C. S. Hutchison, "Ophiolite in Southeast Asia," GSA Bull. **86**, 797–806 (1975).
35. *International Geological Map of Asia. Scale 1 : 5000000* (Comm. Geol. Map World, Inst. Geol., Chinese Acad. Geol. Sci., 2013).
36. International Seismological Centre. ISC-GEM Earthquake Catalogue (2024, Vers. 11). https://doi.org/ (Accessed June 16, 2025). https://doi.org/10.31905/d808b825
37. Kahramanmaraş–Gaziantep Turkey M = 7.7 earthquake, February 6, 2023 (04:17 GMT+03:00) (Boğazici Univ. Kandilli Observ. Sci. Rep., 2023). https://eqe.bogazici.edu.tr/sites/eqe.boun.edu.tr/files/kahramanmaras-gaziantep_earthquake_06-02-2023_04.17-bogazici_university_earthquake_engineering_department_v6.pdf (Accessed June 16, 2025).
38. R. Lacassin, A. Replumaz, and P. H. Leloup, "Hairpin river loops and slip-sense inversion on southeast Asian strike-slip faults," Geology **26**, 703–706 (1998).
39. A. Y. Le Dain, P. Tapponnier, and P. Molnar, "Active faulting and tectonics of Burma and surrounding regions," J. Geophys. Res.: Solid Earth **89**, 453–472 (1984). https://doi.org/10.1029/JB089iB01p00453
40. W. Lei, G. Shi, M. Santosh, Y. Ng, Y. Liu, J. Wang, G. Xie, and Y. Ju, "Trace element features of hydrothermal and inherited igneous zircon grains in a mantle wedge environment: A case study from Myanmar jadeitite," Lithos **266–267**, 16–27 (2016). https://doi.org/10.1016/j.lithos.2016.09.031
41. Y. Lei, A. Gardner, and P. Agram, "Autonomous repeat image feature tracking (auto-RIFT) and its application for tracking ice displacement," Remote Sens. **13** (4), 749 (2021). https://doi.org/10.3390/rs13040749
42. C.-Z. Liu, S.-L. Chung, F.-Y. Wu, C. Zhang, Y. Xu, J.-G. Wang, Y. Chen, and S. Guo, "Tethyan suturing in Southeast Asia: Zircon U–Pb and Hf–O isotopic constraints from Myanmar ophiolites," Geology **44**, 311–314 (2016). https://doi.org/10.1130/G37342.1
43. J. Malpas, M.-F. Zhou, P. T. Robinson, and P. H. Reynolds, "Geochemical and geochronological constraints on the origin and emplacement of the Yarlung–Zangbo ophiolites, Southern Tibet," in *Ophiolites in Earth History*, Ed. by Y. Dilek and P. T. Robinson (Spec. Publ.—Geol. Soc. London, 2003, Vol. 218), pp. 191–206.
44. T. Maurin, F. Masson, C. Rangin, U. T. Min, and P. Collard, "First global positioning system results in northern Myanmar: constant and localized slip rate along the Sagaing Fault," Geology **38**, 591–594 (2010). https://doi.org/10.1130/G30872.1
45. T. Maurin and C. Rangin, "Structure and kinematics of the Indo-Burmese Wedge: Recent and fast growth of the outer wedge," Tectonics **28**, TC2010 (2009). https://doi.org/10.1029/2008TC002276
46. A. Mitchell, S. L. Chung, Thura Oo, T. H. Lin, and C. H. Hung, "Zircon U–Pb ages in Myanmar: Magmatic–metamorphic events and the closure of a neo-Tethys ocean?" J. Asian Earth Sci. **56**, 1–23 (2012). https://doi.org/10.1016/j.jseaes.2012.04.019
47. P. Molnar and J. M. Stock, "Slowing of India's convergence with Eurasia since 20 Ma and its implications for Tibetan mantle dynamics," Tectonics **28**, TC3001 (2009). https://doi.org/10.1029/2008TC002271
48. *Myanmar: Geology, Resources and Tectonics*, Ed. by A. J. Barber, Khin Zao, and M. J. Crow (Geol. Soc. London, Mem., 2017, Vol. 48).
49. B. Oryan, P. M. Betka, M. S. Steckler, S. L. Nooner, E. O. Lindsey, D. Mondal, A. M. Mathews, S. H. Akhter, S. Singha, and Oo Than, "New GNSS and geological data from the Indo-Burman subduction zone indicate active convergence on both a locked megathrust and the Kabaw Fault," J. Geophys. Res.: Solid Earth **128** e2022JB025550 (2023). https://doi.org/10.1029/2022JB025550
50. R. B. Pedersen, M. P. Searle, A. Carter, and P. C. Bandopadhyay, "U–Pb zircon age of the Andaman ophiolite: implications for the beginning of subduction beneath the Andaman–Sumatra arc," J. Geol. Soc. London **167**, 1105–1112 (2010). https://doi.org/10.1144/0016-76492009-151
51. K. A. Raju, T. Ramprasad, P. S. Rao, B. Ramalingeswara Rao, and J. Varghese, "New insights into the tectonic evolution of the Andaman Basin, northeast Indian Ocean," Earth Planet. Sci. Lett. **221**, 145–162 (2004). https://doi.org/10.1016/S0012-821X(04)00075-5
52. J. S. Ray, K. Pande, and R. Bhutani, "$^{40}Ar/^{39}Ar$ geochronology of subaerial lava flows of Barren Island volcano and the deep crust beneath the Andaman Island Arc, Burma Microplate," Bull. Volcanol. **77**, Art. 57 (2015). https://doi.org/10.1007/s00445-015-0944-9
53. A. Replumaz, R. Lacassin, P. Tapponnier, and P. H. Leloup, "Large river offsets and Plio-Quaternary dextral slip rate on the Red River Fault (Yunnan, China)," J. Geophys. Res. **106** (B1), 819–836. https://doi.org/10.1029/2000JB900135
54. L. M. Schoenbohm, B. C. Burchfiel, C. Liangzhong, and Y. Jiyun, "Miocene to present activity along the Red River Fault, China, in the context of continental extrusion, upper-crustal rotation, and lower-crustal flow," GSA Bull. **118**, 672–688 (2006). https://doi.org/10.1130/B25816.1
55. M. P. Searle, C. K. Morley, D. Waters, N. Gardiner, U. Kyi Htun, Than Than Nu, and L. Robb, "Tectonic and metamorphic evolution of the Mogok metamorphic and jade mines belts and ophiolitic terranes of Burma (Myanmar)," in *Myanmar: Geology, Resources and Tec-*

tonics, Ed. by A. J. Barber, Khin Zao, and M. J. Crow (Geol. Soc. London, Mem., 2017, Vol. 48), pp. 261–294. https://doi.org/10.1144/M48.12

56. A. M. C. Sengör, "The Cimmeride orogenic system and the tectonics of Eurasia," GSA, Boulder, USA, GSA Spec. Publ. **195** (1984).
57. R. A. Sloan, J. R. Elliott, M. P. Searle, and C. K. Morley, "Active tectonics of Myanmar and the Andaman Sea," in *Myanmar: Geology, Resources and Tectonics,* Ed. by A. J. Barber, Khin Zao and M. J. Crow (Geol. Soc. London, Mem., 2017, Vol. 48), pp. 19–52. https://doi.org/10.1144/M48.2
58. A. Socquet, C. Vigni, N. Chamot-Rooke, W. Simons, C. Rangin, and B. Ambrosius, "India and Sunda plates motion and deformation along their boundary in Myanmar determined by GPS," J. Geophys. Res.: Solid Earth **111**, B05406 (2006). https://doi.org/10.1029/2005JB003877
59. M. S. Steckler, D. R. Mondal, S. H. Akhter, L. Seeber, L. Feng, J. Gale, E. M. Hill, and M. Howe, "Locked and loading megathrust linked to active subduction beneath the Indo-Burman Ranges," Nat. Geosci. **9**, 615–618 (2016). https://doi.org/10.1038/NGEO2760
60. W. J. Su and A. M. Dziewonski, "Simultaneous inversion for 3D variations in shear and bulk velocity in the mantle," Phys. Earth Planet. Inter. **100**, 135–156 (1997). https://doi.org/10.1016/S0031-9201(96)03236-0
61. A. Todrani, F. Speranza, N. D' Agostino, and B. Zhang, "Post-50 Ma evolution of India–Asia collision zone from paleomagnetic and GPS data: Greater India indentation to eastward Tibet flow," Geophys. Rev. Lett. **49** e2021GL096623 (2021). https://doi.org/10.1029/2021GL096623
62. R. Torres, P. Snoeij, D. Geudtner, D. Bibby, M. Davidson, E. Attema, P. Potin, B. Rommen, N. Floury, N. Brown, I. Navas Trave, P. Deghaye, B. Duesmann, B. Rosich, N. Miranda, C. Bruno, M. L'Abbate, R. Croci, A. Pietropaolo, M. Huchler, and F. Rostan, "GMES Sentinel-1 mission," Remote Sens. Environ. **120**, 9–24 (2012). https://doi.org/10.1016/j.rse.2011.05.028
63. V. G. Trifonov, "Using active faults for estimating seismic hazard," J. Earthquake Predict. Res. **8** (2), 157–184 (2000).
64. H. Tsutsumi and T. Sato, "Tectonic geomorphology of the southernmost Sagaing Fault and surface rupture associated with the May 1930 Pegu (Bago) earthquake, Myanmar," Bull. Seism. Soc. Am. **99**, 2155–2168 (2009). https://doi.org/10.1785/0120080113
65. USGS Earthquake Hazard Program. *M* 7.5–2023 Elbistan Earthquake, Kahramanmaras Earthquake Sequence. https://earthquake.usgs.gov/earthquakes/eventpage/us6000jlqa/executive (Accessed June 16, 2025).
66. USGS Earthquake Hazard Program. *M* 7.7–2025 Mandalay, Burma (Myanmar) Earthquake, Kahramanmaras Earthquake Sequence. https://earthquake.usgs.gov/earthquakes/eventpage/us7000pn9s/executive (Accessed June 16, 2025).
67. D. G. Van der Meer, D. J. Van Hinsbergen, and W. Spakman, "Atlas of the underworld: Slab remnants in the mantle, their sinking history, and a new outlook on lower mantle viscosity," Tectonophysics **723**, 309–448 (2018). https://doi.org/10.1016/j.tecto.2017.10.004
68. P. Vernant, R. Bilham, W. Szeliga, D. Drupka, S. Kalita, A. K. Bhattacharyya, and T. Berthet, "Clockwise rotation of the Brahmaputra Valley relative to India: Tectonic convergence in the eastern Himalaya, Naga Hills and Shillong Plateau," J. Geophys. Res.: Solid Earth **119**, 6558–6571 (2014). https://doi.org/10.1002/2014JB011196
69. C. Vigny, A. Socquet, C. Rangin, N. Chamot-Rooke, M. Pubellier, M. N. Bouin, and M. Becker, "Present-day crustal deformation around Sagaing fault, Myanmar," J. Geophys. Res.: Solid Earth **108** (B11), 2533 (2003). https://doi.org/10.1029/2002JB001999
70. M. Wang and Z. K. Shen, "Present-day crustal deformation of continental China derived from GPS and its tectonic implications," J. Geophys. Res.: Solid Earth **125** e2019JB018774 (2020). https://doi.org/10.1029/2019JB018774
71. Y. Wang, J. B. H. Shyu, K. Sieh, H. W. Chiang, C. C. Wang, Thura Aung, and Soe Thura Tun, "Permanent upper plate deformation in western Myanmar during the great 1762 earthquake: Implications for neotectonic behavior of the northern Sunda megathrust," J. Geophys. Res.: Solid Earth **118**, 1277–1303 (2013). https://doi.org/10.1002/jgrb.50121
72. Y. Wang, K. Sieh, Soe Thura Tun, K. -Y. Lai, and Myint Than, "Active tectonics and earthquake potential of the Myanmar region," J. Geophys. Res.: Solid Earth **119**, 3767–3822 (2014). https://doi.org/10.1002/2013JB010762
73. Yu Wang, Kerry Sieh, Thura Aung, Soe Min, Saw Ngwe Khaing, and Soe Thura Tun, "Earthquakes and slip rate of the southern Sagaing Fault: Insights from an offset ancient fort wall, lower Burma (Myanmar)," Geophys. J. Int. **185**, 49–64 (2011). https://doi.org/10.1111/j.1365-246X.2010.04918.x
74. D. L. Wells and K. J. Coppersmith, "New empirical relationship among magnitude, rupture length, rupture width, rupture area, and surface displacement," Bull. Seism. Soc. Am. **84**, 974–1002 (1994). https://doi.org/10.1785/BSSA0840040974
75. J. W. Yang, Z. Q. Xu, S. D. Duan, Z. Li, F. S. Xyun, Zh. Liu, Zh. H. Zai, and H. Z. Li, "Discovery of a Jurassic SSZ ophiolite in the Myitkyina region of Myanmar," J. Yanshi Xuebao **28**, 1710–1730 (2012). [in Chinese with English abstracts].
76. A. Yin and T. M. Harrison, "Geological evolution of the Himalayan–Tibetan orogen," Ann. Rev. Earth Planet. Sci. **28**, 211–280 (2000). https://doi.org/10.1146/annurev.earth.28.1.211
77. Q. Zhang, Y. Wang, G. Q. Zhou, Q. Qian, and P. T. Robinson, "Ophiolites in China: Their distribution, age and tectonic setting," in *Ophiolites in Earth History*, Ed. by Y. Dilek and P. T. Robinson (*Spec. Publ.—Geol. Soc. London*, 2003, Vol. 218), pp. 541–566.

Publisher's Note. Pleiades Publishing remains neutral with regard to jurisdictional claims in published maps and institutional affiliations.
AI tools may have been used in the translation or editing of this article.